

PREDICTIVE CAPABILITIES OF FINITE ELEMENT MODELLING FOR TIMBER MEMBERS SUBJECTED TO BLAST LOADS

Damian Oliveira¹, Christian Viau², Ghasan Doudak³

ABSTRACT: High-fidelity modelling used to predict the dynamic behaviour in terms of displacement-time history and failure mechanism of heavy timber elements are presented and validated. A material predictive model was implemented in ABAQUS through a dynamic user subroutine using continuum damage mechanics. Full-scale experimental test results were analysed and used to validate the modelling predictions. Compared with the experimental test results, the finite element models simulated the displacement-time histories and overall failure behaviour reasonably well. The accurate prediction of failure modes and overall responses of timber elements, including those with complex properties such as cross-laminated timber, is important to ensure safer designs, and lead to a better overall understanding of the material behaviour when subjected to very short duration loading.

KEYWORDS: Blast, Glulam, CLT, Dynamic, Finite element, Modelling, Failure, Criteria, Resistance, Damage

1 INTRODUCTION

Investigations into wood behaviour under extreme loadings have historically focussed on small-scale clear wood specimens subjected to impact loading. Recent effort in this field has dealt with full-scale structural elements, such as stud walls, glued-laminated (glulam) members, and cross-laminated timber (CLT) panels under simulated blast loading. The validity of using single-degree-of-freedom (SDOF) analysis to predict and investigate the behaviour of full-scale heavy-timber structural elements subjected to blast loading has been extensively investigated [1-3], while the use and application of FEA has been very limited, in part due to the need for material properties that are difficult to isolate and establish experimentally [4].

The continuum damage approach, whereby stress-based criteria are used to initiate the damage process, allows for the detection of both brittle and ductile failure modes, whereas simplified modelling methods, such as SDOF analysis, are typically limited to a single failure mode. The applicability of the SDOF modelling approach has been investigated for wood elements [2, 3, 5-10]. The current study presents and validates a FE modelling approach capable of capturing the behaviour of glulam and CLT elements when subjected to blast loading. Validation of the model is undertaken using published full-scale experimental test results from [11].

2 LITERATURE REVIEW

Analytical and numerical models are often used for the purpose of analysis and design of structural systems due to their low cost and their ability to expand the scope of experimental studies. The most common analysis method

for blast is the equivalent single-degree-of-freedom (SDOF) analysis, which consists of lumping continuous structural elements into a system with given resistance function, equivalent mass, and based on assumed deflected shapes [12]. SDOF analysis has been shown to provide adequate numerical predictions with little required computational efforts [2, 3, 5-10]. However, such simplified modelling techniques are limited to their assumed deflected shape and associated failure mode, and may therefore lead to inconsistencies between modelling predictions and actual sequence of damage or failure events in complex structural systems.

Modelling wood components within a finite element analysis (FEA) environment carries challenges related to properly reproducing the anisotropic nature of the wood material and the interactions between various failure mechanisms. Wood may exhibit brittle and ductile failure mechanisms depending on the failure plane and direction, and such failures may need to be considered simultaneously. While brittle failure modes are typically modelled using fracture mechanics or discrete lattice models, which are capable of capturing detailed property variation [13], ductile failure modes are usually captured using plasticity-based models, such as the Hill criterion [14] and the Tsai-Wu criterion [15].

Continuum damage mechanics-based models [16], whereby elements are modelled as being composed of subdivided areas for the purpose of developing formulations that provide average stress and strains, have been widely implemented in a variety of commercial software packages. Sandhaas, et al. [17] developed a static material model for timber in ABAQUS using solid three-dimensional elements within a continuum damage approach, which allowed for the detection of both brittle and ductile failure modes. The model used stress-based

¹ Damian Oliveira, Canadian Wood Council, Canada, doliveira@cwcc.ca

² Christian Viau, Assistant Professor, Carleton University, Canada, christian.viau@carleton.ca

³ Ghasan Doudak, Professor, University of Ottawa, Canada, gdoudak@uottawa.ca

criteria, each associated with a specific failure mode, to initiate the damage process.

The current study focuses on developing and validating a FEA model based on the continuum damage approach that can predict the behaviour of full-scale wood elements subjected to far-field blast explosions, and their associated strain rate effects. The numerical investigation will focus on glulam and CLT as these are the dominant engineered wood products (EWPs) currently being used for mid- and high-rise wood and hybrid construction.

3 FINITE ELEMENT MODEL

3.1 MODEL DEFINITION

ABAQUS was chosen for the purpose of this study due to its ability to perform both static and dynamic analyses with a variety of element types and applications. An advancing time-step solution, suitable for high-speed dynamic analyses with nonlinear behaviour, was utilized to determine the kinematic state of the model at every time-step. The non-iterative nature of this specific formulation tends to result in less memory usage and runtime.

The models utilized three-dimensional solid geometries without planes of symmetry. Eight-node continuum linear hexahedral elements (C3D8) were used in all analyses and the overall solution algorithm uses a continuum damage approach [4], based on the approach proposed by Sandhaas, et al. [17]. The model was developed following five assumptions, as follows:

1. the adhesive used for bonding the lamination of the timber elements is at least as strong as the surrounding wood fibres and the modelling of the bonds between individual laminations can be omitted;
2. the ultimate compressive behaviour of wood does not result in complete material failure, leading to element deletion from the model environment;
3. damage accumulation in the tension parallel-to-grain direction does not influence damage in other stress components until complete failure;
4. deletion of elements subjected to only shear stresses require not only the exceedance of the failure criterion associated with shear stress, but also additional stresses which would widen the existing cracks in situ, and;
5. the inclusion of the rolling shear component alongside the longitudinal shear component was found to lead to unrealistic and rapid degradation in tension perpendicular-to-grain, and was therefore omitted from any interaction with the tension perpendicular-to-grain stress component.

A total of eight failure criteria are used to represent the state of damage in a given element. The predicted stresses are evaluated using failure criteria which represent the stress-capacity ratios for the element. The respective damage components are identified using specific subscripts: longitudinal tension (t0), longitudinal compression (c0), radial tension (t90R), radial compression (c90R), tangential tension (t90T), tangential compression (c90T), longitudinal shear with respect to the radial plane (vR), and longitudinal shear with respect to the tangential plane (vT). These are presented as follows:

$$F_{t0}(\sigma) = \frac{\sigma_L}{f_{t0}} \quad (1)$$

$$F_{c0}(\sigma) = \frac{-\sigma_L}{f_{c0}} \quad (2)$$

$$F_{c90R|T}(\sigma) = \frac{-\sigma_{R|T}}{f_{c90}} \quad (3)$$

$$F_{t90T|R}(\sigma) = \frac{\sigma_{R|T}^2}{f_{t90}^2} + \frac{\sigma_{LT|LR}^2}{f_v^2} \quad (4)$$

$$F_{vR|T}(\sigma) = \frac{\sigma_{LT|LR}^2}{f_v^2} + \frac{\sigma_{RT}^2}{f_{roll}^2} \quad (5)$$

Each criterion presented above can be considered as a ratio of applied stress (σ) to the material capacity (f). The damage process is initiated if a failure criterion is evaluated to be greater than unity, at which point it is established that an element stress exceeded the elastic limit.

The criterion result of each stress component is then verified against the respective maximum ratio from the previous time steps to determine if damage within the element has progressed. This is performed through the peak stress-history variable, κ , which is used to calculate damage. Depending on the detected failure mode, the damage progression either weakens the element (i.e., brittle tension failure) or allows for sustained stress to take place while the element deforms (i.e., ductile compression failure). In addition, as shear damage can be initialized by other failure criteria, the method of superposition, or coupling, is utilized to capture the complex interactions occurring within the three shear planes (i.e. RT, LR, and LT), as proposed in [18]. For CLT, it is also proposed in the current study that the rolling shear damage variable (d_{roll}) is comprised of the longitudinal shear (d_{vR} and d_{vT}) and perpendicular-to-grain tension (d_{t90R} and d_{t90T}) damage components. The damage equations are presented below:

$$d_t = 1 - \frac{1}{f_{max}^2 - 2G_f E} \left(f_{max}^2 - \frac{2G_f E}{\kappa} \right) \quad (6)$$

$$d_v = 1 - \frac{1}{f_{max}^2 - 2G_f G} \left(f_{max}^2 - \frac{2G_f G}{\kappa} \right) \quad (7)$$

$$d_c = 1 - \frac{1}{\kappa} \quad (8)$$

$$d_{roll} = 1 - (1 - d_{t90R})(1 - d_{t90T})(1 - d_{vR})(1 - d_{vT}) \quad (9)$$

$$d_{vR|T}^{eff} = 1 - (1 - d_{t90R|T})(1 - d_{vR|T}) \quad (10)$$

where d_t is the brittle damage in tension, d_v is the brittle damage in shear, d_c is the ductile damage in compression, and $d_{vR|T}^{eff}$ is the effective shear damage variable.

As seen in Equations (9) and (10), the method of superposition was utilized to capture the complex interactions occurring within the three shear planes (i.e. RT, LR, and LT), as proposed in [18], to calculate shear damages.

Viscous stabilization was incorporated into the damage algorithm through a modification of the damage variables using a bulk viscosity parameter to limit the damage development within the element and prevent large sections of the model from being deleted instantaneously, which is an unrealistic behaviour [4].

The cylindrical axes of wood, namely longitudinal, radial, and tangential, were replaced with the default local cartesian system of reference used within ABAQUS (i.e., X, Y, Z). The behaviour assigned to the perpendicular-to-grain axes within the material was smeared into a homogenized plane, whereby the local longitudinal X-axis was assigned parallel-to-grain properties while identical perpendicular-to-grain properties were assigned to the radial and tangential axes. The stress and strains present within a wood element are therefore defined by a total of six components, as shown in Equation (11) and Equation (12), respectively. These are written using unique properties for the three cartesian axes, but the terms are simplified as the implemented version assigns identical perpendicular-to-grain properties to the Y (denoted R) and Z (denoted T) axes and parallel-to-grain properties to the X (or L) axis. The general constitutive relationship equation includes the elastic modulus parallel-to-grain, E_0 , and perpendicular-to-grain, E_{90} , for the axial components rather than a unique value for each axis, while a longitudinal shear modulus, G , is implemented for both the LR and LT orientations in combination with a rolling shear modulus, G_{roll} , for the RT orientation. The constitutive relationship is presented in Equation (13), while the stiffness matrix of an element, $[k]$, is provided in the literature [4, 19].

$$\{\sigma\} = \{\sigma_L \quad \sigma_R \quad \sigma_T \quad \sigma_{vR} \quad \sigma_{roll} \quad \sigma_{vT}\}^T \quad (11)$$

$$\{\epsilon\} = \{\epsilon_L \quad \epsilon_R \quad \epsilon_T \quad \epsilon_{vR} \quad \epsilon_{roll} \quad \epsilon_{vT}\}^T \quad (12)$$

$$\{\sigma\} = [k]\{\epsilon\} \quad (13)$$

After receiving new incremental strains from the previous step of the ABAQUS analysis, the material model estimates the new stress based on the assumption of linear elastic behaviour. If a damage parameter is evaluated at a value near to unity, the element is identified for deletion.

3.2 TESTING PROGRAM AND MODELLING INPUT

The test configuration and specimens from an experimental study investigating the behaviour of glulam and CLT structural elements subjected to simulated blast loads were utilized for the purpose of validating the finite element model and modelling approach [11]. The experimental testing was conducted using the Shock Tube Test Facility at the University of Ottawa (see Figure 1).



Figure 1: University of Ottawa Shock Tube Test Facility

The specimens, boundary conditions, and loading of ten experimental tests were replicated within the FEA environment and the predicted results (i.e., displacements, reactions, and failure modes) were compared with the experimental test data. The 2,500 mm long specimens consisted of 24f-ES grade glulam beams (86 mm x 178 mm) and E1 grade 5-ply CLT panels (445 mm x 175 mm), subjected to dynamic four-point bending. Strain-rates in the testing varied between 0.10 to 0.32 s⁻¹.

Inputs for the material model pertaining to wood properties were obtained from published manufacturer data and research studies, modified to consider high-strain rate effects. The parallel-to-grain elastic modulus (E_0) was obtained from published design information by the manufacturer. The perpendicular-to-grain modulus of elasticity (E_{90}) and the shear and rolling shear moduli (G and G_{roll} , respectively) were calculated using relationships from the CSA O86 wood design standard [20]. Average strength material properties rather than the design-level properties were obtained from the literature in order to model the in-situ test specimens. The 5th percentile compression and tension parallel-to-grain, as well as perpendicular-to-grain strengths were modified using a load-duration factor (K_D) of 1.25, as well as strength and dynamic increase factors (SIF and DIF). The SIF is used to transform design-level strengths to average static strength values, while the DIF , which is the ratio of the dynamic strength over the static strength, takes into consideration high strain-rate effects [21]. The values for the material properties utilized in the FEA models, including elastic moduli (E), shear moduli (G), strengths (f), fracture energies (G_f), and Poisson's ratios (ν), are summarized in Table 1.

Table 1: Material properties

Property	Glulam	CLT	Ref.
		(Long./Trans.)	
E_0	13,100 MPa	11,700 / 9,000 MPa	[20]
E_{90}	437 MPa	390 / 300 MPa	[20]
G	819 MPa	731 / 563 MPa	[20]
G_{roll}	81.9 MPa	73.1 / 56.3 MPa	[20]
f_{i0}	33.7 MPa	27.7 / 5.8 MPa	[22, 23]
f_{c0}	54.5 MPa	34.7 / 16.2 MPa	[22, 23]
f_{c90}	11.3 MPa	8.0 / 8.0 MPa	[22, 23]
f_{i90}		1.4 MPa	[24]
f_v		10.9 MPa	[25]
f_{roll}		1.5 MPa	[26]
G_{fp}		6.0 N/mm	[4]
G_{fp0}		0.5 N/mm	[4]
G_{fv}		1.2 N/mm	[4]
G_{froll}		0.6 N/mm	[4]
ν_{LR}		0.47	[27]
ν_{LT}		0.37	[27]
ν_{RT}		0.44	[27]

The glulam specimens were modelled as homogenous members, while the plies of the modelled CLT panel were created by portioning sections of the panel geometry. This significantly reduced computational efforts by reducing contact relationships in the analysis. An example of a modelled CLT panel is presented in Figure 2. The boundary supports for the models consisted of four cylindrical rigid bodies, acting as pinned supports, in order to replicate the boundary conditions used during the full-scale experimental tests.

As the validation of the FE model was to be conducted through comparisons with published full-scale test results which utilized a load-transfer device (LTD) to convert the blast pressure into two concentrated point loads, the inertial contribution of the LTD was accounted for by distributing the effective mass of the LTD over the middle third of the member. This was implemented by increasing the material density in the region between the loading areas.

In order to select an appropriate mesh for the finite element material model, an h-refinement based sensitivity analysis was conducted for the glulam and CLT models using a blast load that would induce an elastic response in both specimens. For the purpose of this study, a mesh size of 20 mm was used for the glulam specimens as it provided the highest resolution of results. For the CLT model, considerations were made to include at least two elements for each ply. Overall, the CLT model was found to be more sensitive to mesh size, and a 17.5 mm element size was chosen, since it provided a reasonable balance of result fidelity and runtime.

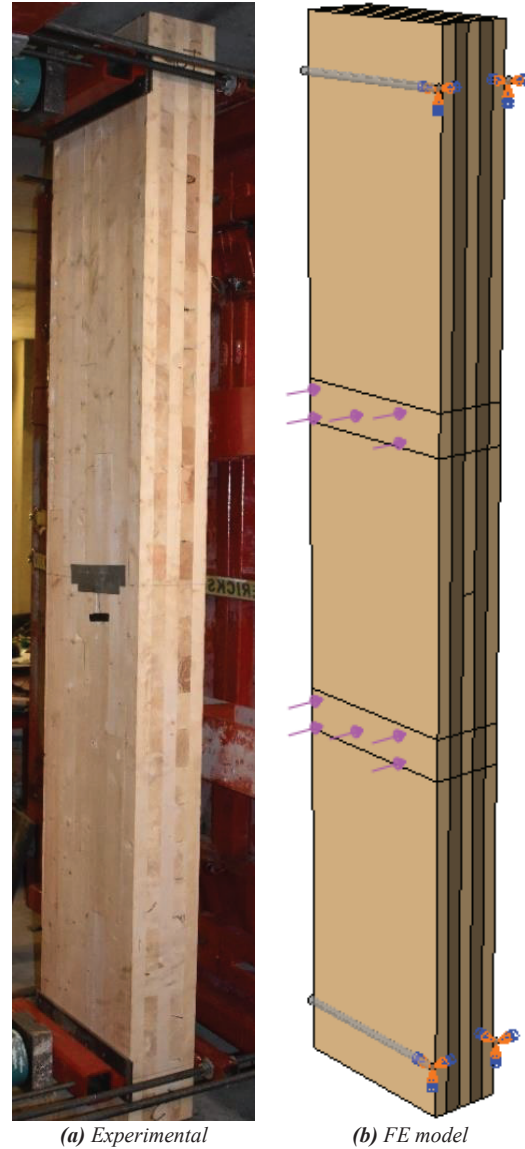


Figure 2: Experimental and numerical CLT specimens

4 RESULTS AND DISCUSSION

The finite element modelling results were evaluated through the displacement-time history and resistance-displacement relationship, as well as the observed overall damage behaviour. The displacement-time history was obtained from a mid-span node, located at mid-depth of the modelled specimen. The numerical results and the corresponding experimental test results are presented in Table 2, which includes the peak resistance and the mid-span displacement occurring at peak resistance.

Table 2: Summary of numerical and experimental results

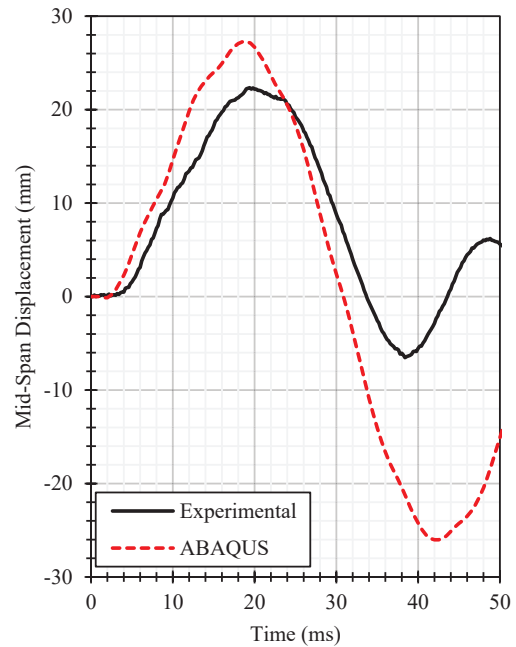
Test Name	Peak Resistance (kN)			Displacement at Peak (mm)		
	Exp.	Num.	Err. (%)	Exp.	Num.	Err. (%)
GL1.1	54	53	-2	26	25	-4
GL2.1	77	61	-21	33	38	+15
GL2.2	79	65	-18	34	42	+24
GL3.1	29	30	+3	13	13	0
GL3.2	66	56	-15	28	28	0
GL3.3	70	63	-10	31	38	+23
CLT1.1	187	188	+1	33	31	-6
CLT2.1	126	150	+19	22	26	+18
CLT2.2	181	170	-6	34	36	+6
CLT3.1	167	176	+5	26	34	+31

The resistance curves and peak resistances were obtained by establishing equilibrium of the dynamic systems, taking into account the dynamic reactions, $V(t)$, imparted blast load, $F(t)$, and mass properties. The closed-form formulation for the resistance at a certain point in time, $R(t)$, is given in Equation (14):

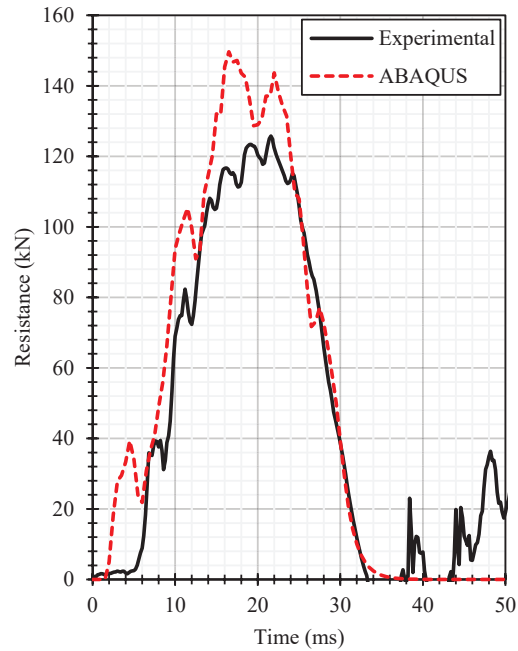
$$R(t) = \frac{6}{L} \left(V(t)x_{eq} + \left(\frac{L}{3} - x_{eq} \right) \frac{F(t)}{2} \right) \quad (14)$$

where L is the clear span of the specimen, and x_{eq} is the location of the equivalent effective inertial force, which can be determined based on previously derived solutions [28]. The reaction-time histories were obtained from the rigid pins in contact with the tension face of the structural elements at the supports.

On average, the model underpredicted the peak resistance by 4.3 % (COV = 12 %) and overpredicted the displacement-at-peak on average by 10.6 % (COV = 11 %). These ratios are well within the expected margins of variability, considering that the inputs were obtained from the timber design standard (CSA O86) [40], manufacturer's data, and studies on similar specimens. Representative experimental and numerical time histories are shown in Figure 3 for specimen CLT2.1. While the model permitted both the inbound and rebound phases of the response to be investigated, the comparison with the experimental test results only extended to the maximum inbound behaviour and response, due to the underlying assumptions involving the LTD mass. While the model considers that the LTD is constantly in contact with the specimen, experimentally this was often not the case, particularly when specimens experienced failure.



(a) Displacement-time



(b) Resistance-time

Figure 3: Representative results (CLT2.1)

The reaction-time histories included numerical scatter due to the solution method used by ABAQUS, which does not calculate the global stiffness or equilibrium. Another potential cause could be attributed to the mismatch between the frequency at which the results from the model outputs are stored and the stable time increment used within the analysis. The stable time increment is related to stress wave propagation velocity within an element, and

thus the output at a certain integration point can vary depending on whether the stress wave has propagated through that specific point of the model at the given time increment.

The FEM results for the glulam specimens matched well in terms of overall deflected shapes and load-displacement behaviour, and propagation of damage through cracks. Failure in the glulam specimens was always initiated on the tension-side outer laminate near the mid-span, corresponding to initial element deletion, followed by damage propagation towards the rest of the cross-section. As shown in Figure 4, the shape and extent of the damage were consistent among simulations and corresponded generally well to the experimental test results.

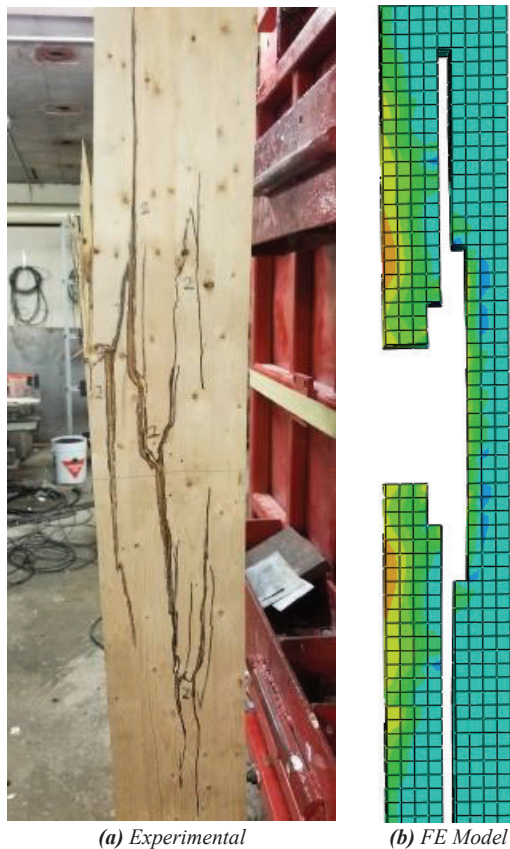


Figure 4: Representative results for glulam

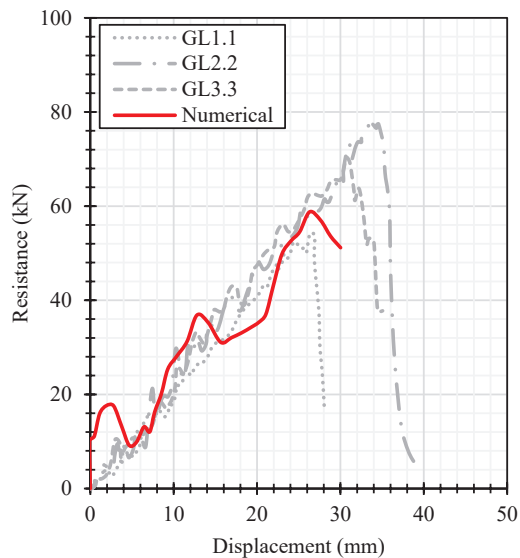
Similar to glulam, the simulated sequence of failure and overall damage characteristics of CLT elements correlated well with those observed in the experimental test specimens, as shown in Figure 5. Two specific failure mechanisms, namely flexural failure of the longitudinal laminates and rolling shear failure of the transverse laminates, were observed experimentally and within the numerical models. This combination of failure modes caused greater variability in terms of the accuracy of the numerical results. However, the FEM consistently predicted rolling shear damage occurring near or at the instance of flexural failure; an observation that was also documented in the experimental tests.



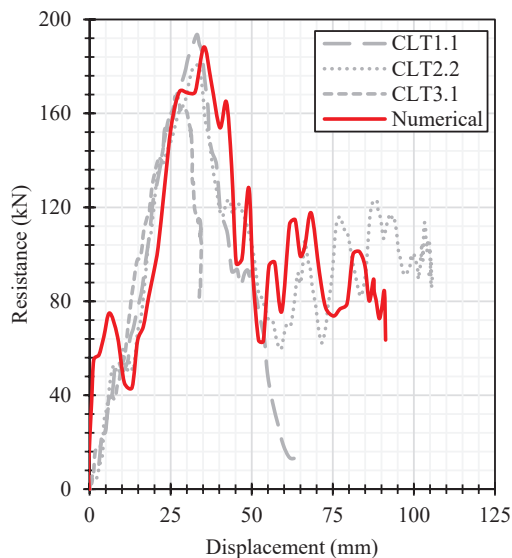
Figure 5: Representative results for CLT

Previous studies on CLT panels under blast have underlined the limitations in the use of simplified SDOF modelling due to the inability of the model to consider two concurrent failure modes [3, 29]. Herein lies the significant advantage of the described ABAQUS model, whereby a multitude of damage types and failure mechanisms can be studied simultaneously, and the output of the model can provide the resistance curve; and input that usually required when performing SDOF analysis.

The resistance curves generated by the finite element method generally correlated well with experimental results despite the presence of artificial numerical fluctuation, as shown in (Figure 6).



(a) Glulam



(b) CLT

Figure 6: Comparison between experimental and numerical resistance curves

The overall numerical results in terms of resistance curve within the elastic regime were very consistent with the experimental test results, with the exception that a very high initial stiffness was observed in all models within the first two milliseconds. This phenomenon does not, however, affect the overall accuracy and results from the FEA model. In both the experimental and numerical results, no post-peak behaviour was observed for the glulam specimens, as shown in Figure 6a, while the CLT specimens exhibited significant post-peak capacity, as shown in Figure 6b. The loss of the outermost longitudinal laminates corresponded with the peak resistance of the panel.

5 CONCLUSIONS

A material predictive model for glued-laminated and cross-laminated timber structural elements was implemented into ABAQUS/Explicit through a dynamic user subroutine following a continuum damage approach. The experimental test results of 10 full-scale shock tube tests were used to validate the accuracy of the model, which was determined to be effective in capturing the dynamic response of timber elements. Reasonably accurate numerical predictions were obtained for peak resistance, as well as mid-span displacements at peak resistance. The finite element models were also capable of predicting damage and failure in the specimen, similar to those observed experimentally. The FE model was found to produce resistance-displacement relationships which correlated well to the corresponding experimental results. This finding identifies a key advantage to using sophisticated FEA over simplified modelling methodologies, such as single-degree-of-freedom modelling. While the latter requires that the resistance curve as input, the former produces the resistance curve, given appropriate material properties are implemented by the analyst. The modelling results also show that the lack of actual in-situ material properties does not pose a challenge in obtaining realistic predictions of overall behaviour and resistance curves, as published data from available manufacturer spec sheets, design provisions, and published studies can be used to obtain generally good results.

REFERENCES

- [1] Jansson, B., *Impact loading of timber beams*, MSc Thesis, 1992, University of British Columbia: Vancouver, BC.
- [2] Lacroix, D.N. and G. Doudak, *Determining the Dynamic Increase Factor for Glued-Laminated Timber Beams*. Journal of Structural Engineering, 2018. 144(9): p. 04018160.
- [3] Poulin, M., C. Viau, D.N. Lacroix, and G. Doudak, *Experimental and Analytical Investigation of Cross-Laminated Timber Panels Subjected to Out-of-Plane Blast Loads*. Journal of Structural Engineering, 2018. 144(2): p. 04017197.
- [4] Sandhaas, C., *Mechanical behaviour of timber joints with slotted-in steel plates*, Doctoral Dissertation, 2012, TU Delft.
- [5] Viau, C. and G. Doudak, *Investigating the Behavior of Light-Frame Wood Stud Walls Subjected to Severe Blast Loading*. Journal of Structural Engineering, 2016. 142(12): p. 04016138.
- [6] Viau, C., D.N. Lacroix, and G. Doudak, *Damage level assessment of response limits in light-frame wood stud walls subjected to blast loading*. Canadian Journal of Civil Engineering, 2016. 44(2): p. 106-116.
- [7] Lacroix, D. and G. Doudak, *Towards enhancing the post-peak performance of glued-laminated timber beams using multi-directional fibre reinforced polymers*. Engineering Structures, 2020. 215: p. 110680.
- [8] Lacroix, D.N. and G. Doudak, *Effects of High Strain Rates on the Response of Glulam Beams and Columns*.

- Journal of Structural Engineering, 2018. 144(5): p. 04018029.
- [9] Lacroix, D.N. and G. Doudak, *Investigation of Dynamic Increase Factors in Light-Frame Wood Stud Walls Subjected to Out-of-Plane Blast Loading*. Journal of Structural Engineering, 2015. 141(6): p. 04014159.
- [10] Lacroix, D.N., G. Doudak, and K. El-Domiati, *Retrofit Options for Light-Frame Wood Stud Walls Subjected to Blast Loading*. Journal of Structural Engineering, 2014. 140(4): p. 04013104.
- [11] Oliveira, D., C. Viau, and G. Doudak, *Behaviour of mass timber members subjected to consecutive blast loads*. International Journal of Impact Engineering, 2023. 173: p. 104454.
- [12] Biggs, J.M., *Introduction to Structural Dynamics*. 1964, New York, NY: McGraw-Hill. 341.
- [13] Reichert, T., *Development of 3d lattice models for predicting nonlinear timber joint behaviour*, 2009, Edinburgh Napier University: Edinburgh, UK.
- [14] Hill, R. and E. Orowan, *A theory of the yielding and plastic flow of anisotropic metals*. Proceedings of the Royal Society of London. Series A. Mathematical and Physical Sciences, 1948. 193(1033): p. 281-297.
- [15] Tsai, S.W. and E.M. Wu, *A General Theory of Strength for Anisotropic Materials*. Journal of Composite Materials, 1971. 5(1): p. 58-80.
- [16] Matzenmiller, A., J. Lubliner, and R.L. Taylor, *A constitutive model for anisotropic damage in fiber-composites*. Mechanics of Materials, 1995. 20(2): p. 125-152.
- [17] Sandhaas, C., J.W.G.V.D. Kuilen, and H.J. Blass, *Constitutive model for wood based on continuum damage mechanics*, in *World Conference on Timber Engineering*. 2012: Auckland, NZ.
- [18] Sandhaas, C., A.K. Sarnaghi, and J.-W. van de Kuilen, *Numerical modelling of timber and timber joints: computational aspects*. Wood Science and Technology, 2020. 54(1): p. 31-61.
- [19] Chen, Z., D. Tung, and E. Karacabeyli, *Modelling Guide for Timber Structures*, in *Special Publication SP-544*. 2022, FPInnovations: Pointe-Claire, Que.
- [20] CSA, *Engineering design in wood*, in *CSA O86*. 2019, CSA Group: Mississauga, ON.
- [21] Doudak, G., C. Viau, and D.N. Lacroix, *Proposed Design Methods for Timber Members Subjected to Blast Loads*. Journal of Performance of Constructed Facilities, 2022. 36(3): p. 04022020.
- [22] Nordic Structures, *Nordic X-Lam Technical Guide*. 2022, Nordic Structures: Montreal, QC.
- [23] Nordic Structures, *Nordic Lam+ Technical Guide*. 2022, Nordic Structures: Montreal, QC.
- [24] Jönsson, J. and S. Thelandersson, *The effect of moisture gradients on tensile strength perpendicular to grain in glulam*. Holz als Roh- und Werkstoff, 2003. 61(5): p. 342-348.
- [25] Boström, L.A., *Method for determination of the softening behaviour of wood and the applicability of a nonlinear fracture mechanics model*. Report TVBM, 1992.
- [26] Wang, Z., J. Zhou, W. Dong, Y. Yao, and M. Gong, *Influence of technical characteristics on the rolling shear properties of cross laminated timber by modified planar shear tests*. Maderas. Ciencia y tecnología, 2018. 20: p. 469-478.
- [27] Green, D.W., J.E. Winandy, and D.E. Kretschmann, *Mechanical properties of wood*. Wood handbook : wood as an engineering material, in *General technical report FPL ; GTR-113*. 1999, USDA Forest Service, Forest Products Laboratory: Madison, WI.
- [28] Lacroix, D., *Investigating the Behaviour of Glulam Beams and Columns Subjected to Simulated Blast Loading*, PhD Dissertation, 2017, University of Ottawa: Ottawa, ON. p. 294.
- [29] Viau, C., D. Lacroix, and G. Doudak, *Design Considerations for Cross-Laminated Timber Panels Subjected to Simulated Blast Loads*, in *CSCE 2018 Annual Conference*. 2018, Canadian Society for Civil Engineering: Fredericton, NB.